Fatigue behavior of additively manufactured Ti3Al2V alloy

Amit Bandyopadhyay, Sushant Ciliveri, Stefano Guariento, Nathan Zuckschwerdt, and William W. Hogg

W. M. Keck Biomedical Materials Research Laboratory,

School of Mechanical and Materials Engineering,

Washington State University, Pullman, WA 99164, USA

Corresponding author: Amit Bandyopadhyay (amitband@wsu.edu)

Abstract

This study measured the tensile, compression, and fatigue behavior of additively manufactured Ti3Al2V as a function of build orientation. Ti3Al2V alloy was prepared by mixing commercially pure titanium (CpTi) and Ti6Al4V in 1:1 wt. ratio. Laser powder bed fusion (L-PBF) based additive manufacturing (AM) technique was used to fabricate the samples. Tensile tests resulted in an ultimate strength of 989 ± 8 MPa for Ti3Al2V. Ti6Al4V 90º orientation samples showed a compressive yield strength of 1178 ± 33 MPa, and that for Ti3Al2V 90º orientation was 968 ± 24 MPa. Varying the build orientation to account for anisotropy, Ti32-45º and Ti32-0º displayed similar compressive yield strength values of 1071 ± 16 and 1051± 18 MPa, respectively, higher than Ti32-90º. Fatigue loading revealed an endurance limit (10 million cycles) of 250 MPa for Ti6Al4V and 219 MPa for Ti3Al2V built at 90° orientations. The effect of the build orientation was significant under fatigue loading; Ti3Al2V built at 45° displayed an endurance limit of 387.5 MPa, and 0° showed 512 MPa; more than two-fold increment in endurance limit was observed. Our results show the potential of Ti3Al2V alloy for orthopedic devices, replacing Ti6Al4V alloy, particularly in load-bearing applications.

Keywords: Additive manufacturing; Titanium alloys; Alloy design; Load-beating implants; Fatigue behavior.

1. Introduction

The critical factors in metallic biomaterial selection include mechanical properties, cytotoxicity, corrosion resistance, and biocompatibility. Titanium (Ti) alloys are the most popular choice for load-bearing implant applications among metallic biomaterials [1], [2]. Commercially pure titanium (CpTi) shows no cytotoxicity and excellent corrosion resistance, popularizing it for over six decades as a first-generation Ti-based biomaterial [3]. Implant devices for hard tissue replacement at load-bearing sites demand high strength and excellent fatigue resistance. CpTi exhibits poor fatigue performance. The ideal replacement was found in aerospace materials: an alloy Ti6Al4V designed by the Army Research Laboratory in the 1950s to achieve high-temperature oxidation resistance for jet engines [4]–[6]. Ti6Al4V shows high strength and excellent fatigue resistance compared to CpTi. Despite Ti6Al4V demonstrating lower biocompatibility than CpTi [7], [8], Ti6Al4V alloy has been employed as the ultimate orthopedic implant material of choice over the past six decades [5], [9]–[12].

Along with promising mechanical performance, biocompatibility also plays a vital role in the implant's stability and longevity [13]. Improper implant fixation is one of the major issues causing the need for revision surgery procedures. Delayed tissue growth, implant surface integration, and host bone attachment are attributed to the material biocompatibility [14]. Since Ti6Al4V does not aid in accelerated bone healing [13], elderly patients with compromised bone health often face the issue of implant loosening. Revision surgery procedures on such patients severely affect their health and may ultimately reduce their life expectancy. To account for the

poor biocompatibility of α+β phase Ti6Al4V, the design and development of various high-strength-low-modulus β-Ti alloys with a relatively higher fraction of a variety of biocompatible β stabilizers such as Mo, Nb, Ta, Fe, Cr, Zr, have been reported [3], [15], [16]. Although these β-Ti alloys exhibited superior biological performance, they lacked fatigue strength compared to Ti6Al4V, making them less than ideal for most load-bearing applications [17]–[19]. Lin et al. demonstrated the fatigue strength of commercial Ti-13Nb-13Zr [20] and Ti-7.5Mo [21] β–Ti alloys to be poorer than both Ti6Al4V and CpTi [17]. The search for a suitable Ti-alloy with enhanced biocompatibility and adequate mechanical performance, especially fatigue strength, persists.

An implant surgically placed *in vivo* at a load-bearing site is constantly under cyclic loading conditions. Fatigue being the dominant means of mechanical failure [22], fatigue resistance is one of the critical parameters determining the implant's longevity [23]. Since β-Ti alloys show poorer fatigue performance [3], a different approach to alloy design must be implemented. Instead of exploring the β-Ti alloy development, we decided to dive into the roots of Ti6Al4V alloy development and stay in the α+β-Ti phase domain. The Al and V alloying elements result in high strength and excellent fatigue resistance in Ti6Al4V. This alloy was not explicitly designed for orthopedic applications but borrowed from the aerospace sector. As discussed, CpTi shows better biocompatibility than Ti6Al4V. A question arises: do we need 6 and 4 wt.% of Al and V in Ti6Al4V for orthopedic applications?

This study employs a novel approach to alloy design: an alloy Ti3Al2V with reduced Al and V contents. An intermediate alloy between CpTi and Ti6Al4V is expected to enhance the biocompatibility without significant degradation in strength. This study is focused on exploring the mechanical performance of this Ti3Al2V alloy, especially the fatigue behavior. This alloy

was designed by mixing CpTi and Ti6Al4V in 1:1 weight ratio. This composition was processed via laser powder bed fusion (L-PBF) based additive manufacturing (AM) technique. AM offers higher degrees of processing freedom over conventional methods and the flexibility of designing novel alloys in complex shapes and sizes [24]–[26]. AM aids in mimicking the patient's bone into the implant to be surgically placed, significantly reducing post-operative complications [27], [28]. Since AM is a layer-wise process, the anisotropy parameter is crucial for the mechanical performance of AM parts under fatigue loading [10]. In this study, Ti3Al2V was fabricated in three orientations, 45- and 90˚, to the build surface for compressive and fatigue characterization.

2. Materials and Methods

2.1 Fabrication via laser powder bed fusion (L-PBF)

Samples were designed on 3DXpert CAD Software (3D Systems, Rock Hill, SC). Compression and fatigue samples were designed and processed with 0, 45, and 90˚ orientations to the build direction, as shown in **Fig. 1**. Fabrication was carried out using L-PBF-based AM technique on a powder bed fusion (PBF) system (3D Systems ProX® DMP 200, Rock Hill, SC) consisting of a fiber laser (300 W) and wavelength λ=1070nm. Commercially pure Ti (CpTi) and Ti6Al4V (Ti64) powders were procured from AP&C (GE Additive, Cincinnati, Ohio, USA) and GKN Hoeganaes (Cinnaminson, NJ), respectively. Ti3Al2V (Ti32) composition was prepared by mixing CpTi and Ti64 in 1:1 weight ratio. All powders were spherically shaped and sieved to obtain a particle size < 63µm. The powders were loaded in the PBF system supply chamber and purged with argon atmosphere to obtain an O_2 < 500 ppm. A CpTi build plate of 2.5 cm thickness was secured on the build platform. The printing operation was carried out with a layer thickness of 30 µm, laser power of 180 W, and scan speed of 1600 mm/s.

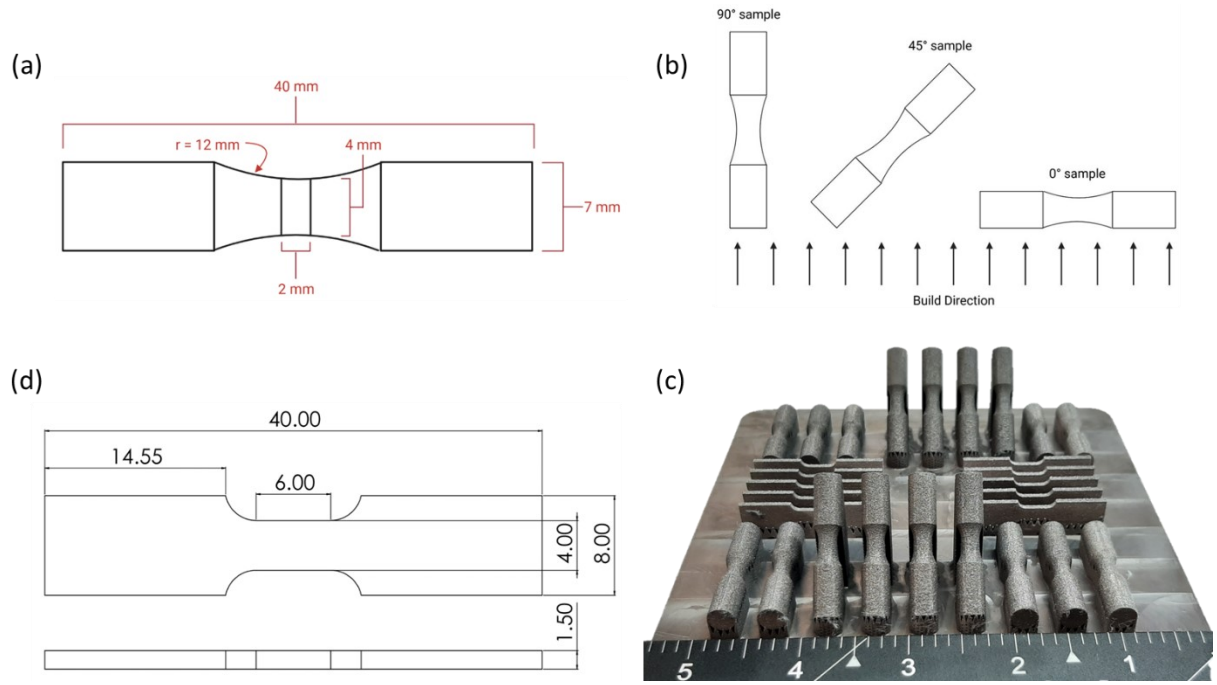

Fig. 1. (a) Dimensions of the fatigue samples designed and printed via L-PBF-based AM technique, and (b) a schematic of different orientations - 0˚, 45˚, and 90˚ to the build plate used for printing and testing the fatigue samples. (c) Dimensions of the tensile test coupons designed and printed via L-PBF. (d) The photo of the build plate post-printing process completion shows fatigue specimen at 0˚ and 45˚ orientations to the build plate and tensile specimens.

2.2. Post-Processing – Fatigue specimens

Fatigue samples were subjected to identical post-processing steps to ensure consistent and reproducible results during subsequent analyses. These steps included turning, heat treating, and sanding the samples before fatigue testing. Ti32 0˚ and 45˚ samples processed via PBF were printed with support layers positioned beneath the cylindrical surfaces, unlike their 90-degree counterparts. Prior to performing surface smoothing actions, it was necessary to eliminate the support structures. This task was accomplished using pliers and a vice grip to pry the supports off. This procedure and the prints themselves gave rise to minor deformation in the samples,

which resulted in non-concentric samples. Tormach 770MX (Tormach Inc., Monona, WI) CNC machine with a rapid turn feature was utilized to remove sufficient material from the samples until they were concentric and free of any deformation to address this issue. A pilot hole was drilled in the other end of the sample and fit with a live center to improve rigidity when turning.

The initial steps were to achieve a smooth surface finish on the 0˚ and 45˚ samples, which involved Autodesk Fusion 360 and the Tormach 770MX. The sample would then be gripped by one end in the chuck while the other is supported concentrically using a center point tool in the tailstock. This step is necessary for all the 0- and 45-degree samples to ensure concentric rotation. Using the CNC machine, the carbide insert tool removed 0.1 mm radius from the sample during each pass. Multiple passes would be made gradually until the surface of the fatigue sample was visually smooth. For all Ti32 0-, 45-, and 90-degree samples, this same Tormach surface smoothing process was followed. Once the samples were turned and processed, the next step was to remove the overhanging metal initially secured in the chuck of the CNC machine. When turning the fatigue samples, part of the metal must be secured in the chuck to ensure a strong grip is held on the part. This extra piece of metal was removed using a bandsaw. Once removed, the sample was placed in a Thermolyne 48000 furnace at 400˚ C for one hour. The sample would then be furnace-cooled for 12 h. Finally, once heat treated, the sample is placed in a drill press, and the gauge and stems are sanded down using 400 – 600 grit emery cloth until all visual defects are nonexistent.

2.3. Microstructural characterization

The top surface of the fatigue specimens was cut and mounted in a phenolic resin. The samples were ground through 80-1200 SiC grit-size grinding papers and polished using alumina dispersed in deionized water with particle size gradually reducing from 1-0.05 μm. The samples

were etched in Kroll's reagent, and the microstructure was acquired on a Keyance digital microscope (Model VHX-7000, Itasca, IL).

2.4. Tensile and compression tests

Dog-bone-shaped samples were mounted using manual non-shift wedge grips in a Shimadzu AG-1S Precision Universal Tensile Tester (Shimadzu, Columbia, Maryland). The samples were tested till failure using a constant crosshead displacement rate of 0.75 mm/min displacement, and the raw load vs. displacement data was recorded. All samples used were made following ASTM 52909 [29, p. 52] guidelines for the sizing of the sample, leading to a designed size of a 6 mm gauge length and a cross-sectional area of 4 mm by 1.5 mm. For the heat treatment of the samples, they were placed in a furnace at 400˚ C for 1 h, and then furnace cooled. The fracture surface of the tensile specimens was observed under a field emission Scanning Electron Microscope (FESEM, FRI-SIRION, Portland, OR). Dense samples fabricated via L-PBF with a diameter of 7 mm and ~15 mm height were used for compression tests. Ti64 samples used were built at a 90˚ orientation. For Ti32, the samples tested were built in 0, 45, and 90˚ orientations to the build plate. The samples were tested on an Instron servohydraulic system (600DXS, Grove City, Pennsylvania) following ASTM E9-19 [30]. A 1.3 mm/min crosshead displacement rate was used, and the raw load vs. displacement data was recorded. Compressive yield strength was evaluated from the raw data using the 0.2% strain offset method. Each composition and orientation had at least 3 replicates tested.

2.5. Fatigue test

The post-processed samples were subjected to cyclic loading on an ADMET (Norwood, MA) Rotating Beam Fatigue Test System (4-point loading) fitted with Tormach (Madison,

Wisconsin) 6mm ER32 collets, in accordance with ISO 1143 [31]. The gauge length of the test specimens was cleaned with ethanol. The system applies a load calculated from the stress amplitude and measured gauge diameter. The stress amplitude used was calculated as,

$$S = F\frac{32L}{\pi d^3}$$

where F is the bending force applied, L is the force arm length, and d is the gauge diameter. The loads selected were presented as the ratio of the bending load applied and their respective compressive yield strength, **Table 3**. Once the set load is applied, the sample is rotated at 3000 rpm until fracture or reaches 10 million cycles without fracture at a stress amplitude of S and a stress ratio of R = -1 for pure reverse stress-controlled loading. The endurance limit was the lowest bending stress at which samples reached 10 million cycles without fracture. Post fracture, the fracture surfaces were observed under a Keyance digital microscope (Model VHX-7000, Itasca, IL).

3. Results

Ti6Al4V alloy is widely used for orthopedic implants owing to its excellent strength and fatigue performance. It exhibits poorer biological performance than CpTi, which lacks strength requirements. The enhanced strength in Ti6Al4V alloy is because of the alloying elements Al and V, the primary purpose was to achieve high-temperature oxidation for aerospace applications. Since high-temperature oxidation is not a requirement for orthopedic implants, a novel alloy, Ti3Al2V, with reduced Al and V in Ti6Al4V, has been designed and developed specifically for orthopedic applications. We hypothesize that Ti32 alloy will demonstrate comparable fatigue resistance and strength performance to Ti64.

3.1. Microstructure and build orientation

Fig. 2 reports the microstructures for Ti64-90 and Ti32 at 0-45-90° build orientations. All samples show typical metastable α' martensitic needle-like morphology on the surface, typically observed in additively manufactured Ti64. Ti32-90 displays residual pores on the surface, indicating interlayer lack of fusion; the top surface where the microstructure is observed is perpendicular to the build direction. These residual pores are minimal in Ti32-45 and Ti32-0 since the top surface lies at an angle to the build direction. The effect of this interlayer lack of fusion pores can be observed later in their respective fatigue performance.

3.2. Static mechanical performance - Tensile and compression behavior

Fatigue deformation primarily consists of alternating tensile and compression loading. It is essential to understand the behavior of Ti32 under static tensile and compression loading before fatigue tests. Extensive studies have been carried out to evaluate the tensile performance of Ti64 alloy (**Table 1**). In this study, Ti32 alloy was subjected to tensile tests to evaluate the stress at failure, **Table 2**. As-printed non-heat-treated tensile specimens displayed a tensile elastic modulus of 106.8 ± 4.8 GPa, close to that of Ti6Al4V. Since Ti32 was designed with CpTi and Ti64 concoction in 1:1 weight ratio, and both CpTi and Ti64 display an elastic modulus of 110-114 GPa, the tensile modulus of Ti32 was observed within a similar range. The ultimate tensile strength of non-heat treated Ti32 test specimens was 989 ± 8 MPa, which is quite similar to that of Ti64 900-1200 MPa from various studies, as shown in **Table 1**. AM-processed structures show high strains due to their fast heating and cooling nature. Heat treatment was carried out to relieve the AM process-induced residual stresses.

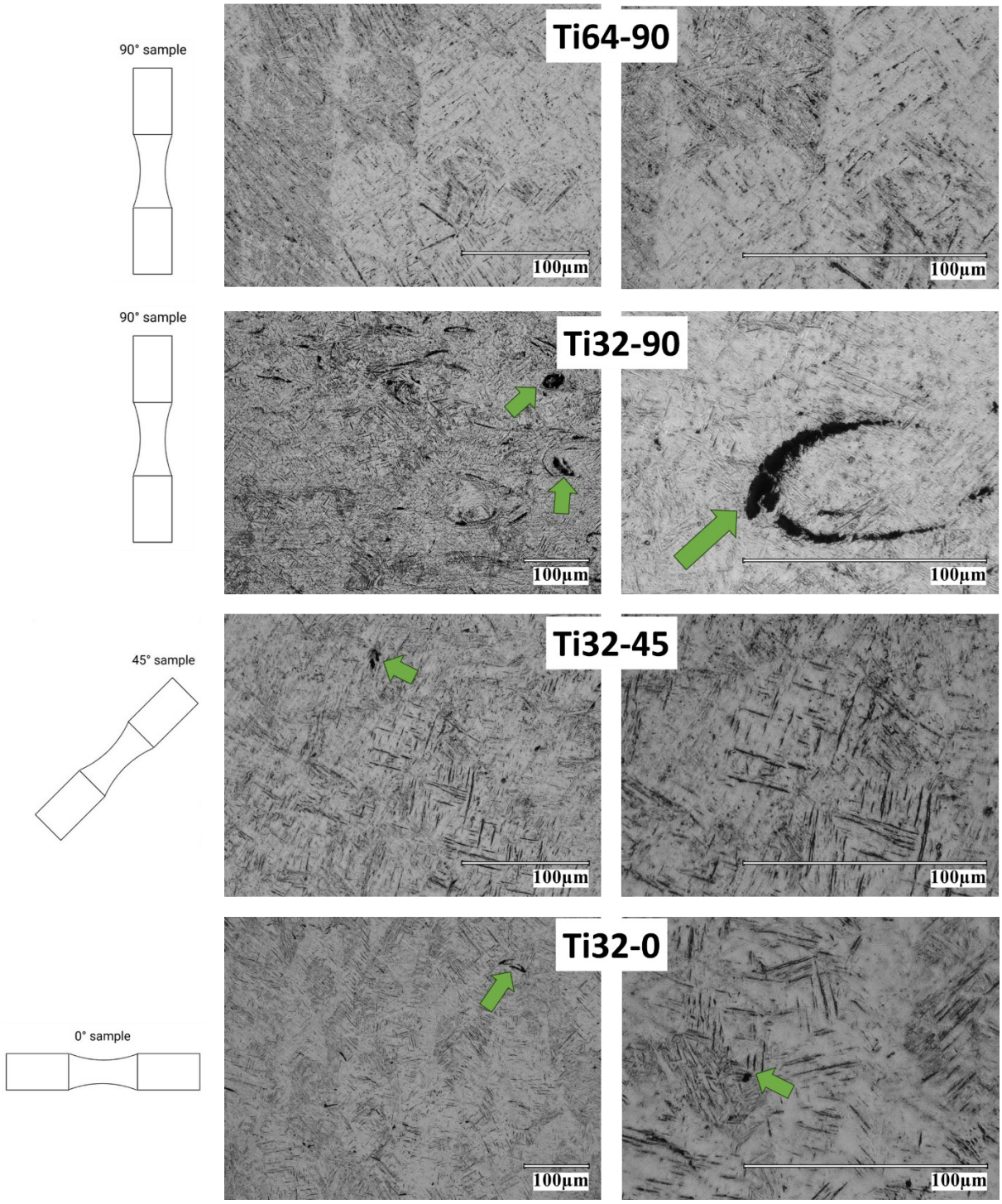

Fig. 2. Microstructures of Ti64-90 and Ti32-90, Ti32-45, and Ti32-0 samples observed on their top surface. α' martensitic needle-like morphology is observed in all specimens. The top surface of the Ti32-90 perpendicular to the build direction exhibits large residual pores. Ti32-45 and Ti32-0 show comparatively lower residual pores.

The tensile elastic modulus of the heat-treated Ti32 specimens was 107.6 8 ± 5.8 GPa, similar to that of non-heat-treated specimens. The ultimate tensile strength was found to be 989 ± 4 MPa and similar to that of the non-heat-treated specimens, suggesting no effect of the heat treatment on the tensile behavior. ISO 5823-3 (implants for surgery metallic materials) dictates the tensile strength requirement for Ti64 to be at least 860 MPa [32]. The tensile strength of Ti32 specimens exceeds this minimum strength requirement. **Fig. 3**. reports the microstructure of the fractured surfaces from tensile tests for Ti32. Micrographs reveal dimple ridges suggesting ductile behavior in conjunction with the elongation of the specimen being 8 ± 2% after failure. All samples fractured at 45°to the loading direction. No effect of heat treatment was observed.

Table 1. The tensile modulus and ultimate tensile strength of Ti6Al4V were processed via directed energy deposition (DED), electron beam melting (EBM), and laser powder bed fusion (L-PBF) based AM techniques from various studies.

AM technique	Post-processing	Tensile modulus (GPa)	Ultimate tensile strength (MPa)	Reference
DED	Machined	-	1041-1087	[33]
	Annealed at 600˚C for 2 h	95.1	907	[34]
	As printed	-	761-821	[35]
	Machined	-	1163	[36]
EBM	Machined	-	1073	[37]
	Machined	-	972	[38]
	As printed	-	851	[39]
	Machined	119	1045	[40]
L-PBF	Annealed at 950˚C for 30 mins, machined	118	1042	[41]
	Machined	110	1095	[42]
	Machined	-	1246	[38]
	Annealed at 730˚C for 2 h, machined	101	1046	[43]
	Annealed at 640˚C for 4 h, machined	127	1032	[40]

Table 2. Tensile test results for heat-treated and non-heat-treated specimens, and compressive yield strength for Ti64 and Ti32 with different build orientations.

TENSILE		
	Elastic modulus (GPa)	**Ultimate tensile strength (MPa)**
Non-Heat-treated Ti32	106.8 ± 4.8	989 ± 8
Heat-treated Ti32	107.6 ± 5.8	989 ± 4
COMPRESSION		
Nomenclature	**Build orientation**	**Compressive yield strength (MPa)**
Ti6Al4V		
Ti64-90	90°	1178 ± 33
Ti3Al2V		
Ti32-90	90°	968 ± 24
Ti32-45	45°	1071 ± 16
Ti32-0	0°	1051 ± 18

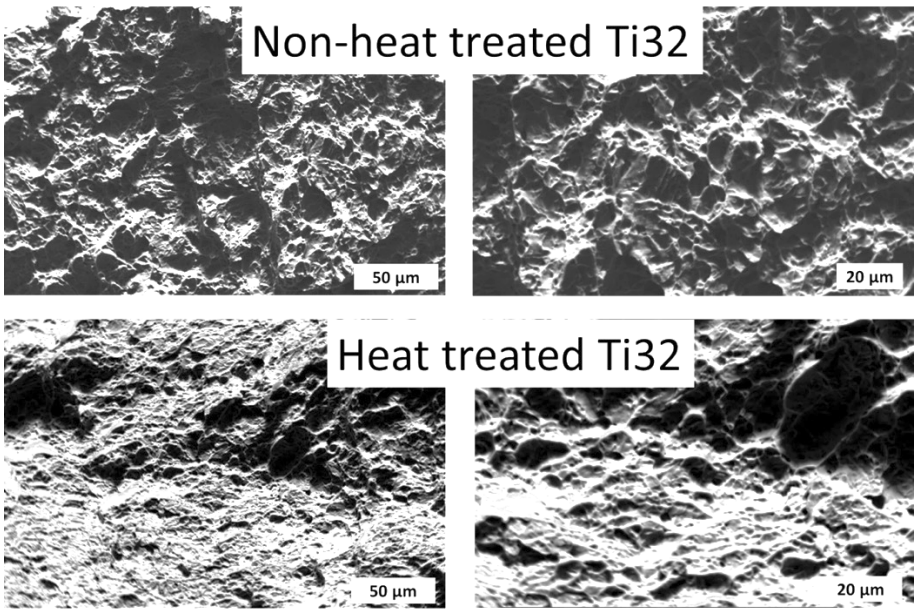

Fig. 3. Fracture surfaces of Ti32 tensile test specimens for non-heat-treated and heat-treated conditions.

Anisotropy is an essential consideration while evaluating the mechanical properties of AM-processed structures. Compression tests were carried out for Ti64 built at 90˚ to the build plate and Ti32 built in three orientations: 0, 45, and 90˚, and the respective compressive yield strengths are presented in **Table 2**. Compositional variation from Ti64 to Ti32 displayed a reduction in compressive yield strength due to lower Al and V alloying elements in Ti32. Ti64-90 showed a compressive yield strength of 1178 ± 33 MPa, and that for Ti32-90 was 968 ± 24 MPa. An effect of the build orientation was observed in the compressive yield strength; compressive yield strength was observed to increase with the reduction in built angle. Ti32-45 and Ti32-0 displayed similar compressive yield strength values of 1071 ± 16 and 1051± 18 MPa, respectively, higher than Ti32-90.

3.3. Dynamic mechanical loading – rotating-bending fatigue

The fatigue performance is expected to deteriorate with a reduction in the Al and V contents in Ti64 to make Ti32. The standard dictates at least 10 million cycles before failure for a composition to qualify as an orthopedic device material. In this study, the endurance limit was considered the bending stress at which the fatigue specimens reached 10 million cycles without failure. **Table 3** reports the cycles till failure for Ti64 and Ti32, and **Fig. 4** reports the plot for the same, along with the fracture surface morphology. With a compressive yield strength of 1178 MPa for Ti64, its high cycle fatigue reached 10 million cycles at 250 MPa at a stress ratio of 0.21 for additively manufactured Ti64-90 specimens. Comparatively, for Ti32-90 with lower Al and V contents, the 10 million cycle mark was achieved at a lower stress of 219 MPa; however, it is to be noted that the stress ratio was 0.22, similar to that of 0.21 for Ti64-90.

Additive manufacturing is a layer-wise process that results in anisotropy, leading to variation in the mechanical performance depending on the build orientation. Along with the

compressive strength, the fatigue performance exhibits the effect of the build orientation. For Ti32-45, 10 million cycles are reached at a stress ratio of 0.36 (bending stress 387.5), higher than that for both Ti64-90 and Ti32-90 test specimens. With a further decrease in the build orientation, Ti32-0 displays 10 million cycles for an even higher stress ratio of 0.48 (bending stress 512.5 MPa). Thus, with a change in build orientation from 90° to 0°, Ti32 shows better fatigue performance than Ti64, compensating for the reduced amounts of Al and V in the former. **Fig. 4b** shows the fracture surface morphologies for Ti64-90 and Ti32-90/45 specimens. The fracture initiates at the surface of the specimens under fatigue loading, which can be observed in the images and propagates throughout the specimen, leading to ultimate failure. This suggests that the surface properties greatly influence their fatigue performance.

Table 3. Fatigue results for Ti64 and Ti32 compositions built at different orientations.

Composition	Orientation	Nomenclature	Compressive yield stress (MPa)	Stress Amplitude (MPa)	Stress ratio (Stress Amplitude/Compressive yield strength)	Cycles
Ti64	**90°**	**Ti64-90**	**1178**	387.5	0.33	19,275
				300	0.25	25,039
						87,147
				250	0.21	10 million*
Ti32	**90°**	**Ti32-90**	**968**	387.5	0.40	2,385
						1,930
				339.94	0.35	10,355
						1,352
				219.318	0.23	10 million*
	45°	**Ti32-45**	**1071**	512.5	0.48	3,993,108
						4,907,598
				450	0.42	10 million*
						6,263,225
				387.5	0.36	10 million*
	0°	**Ti32-0**	**1051**	512.5	0.49	10 million*
						10 million*
				450	0.43	10 million*
				387.5	0.37	10 million*

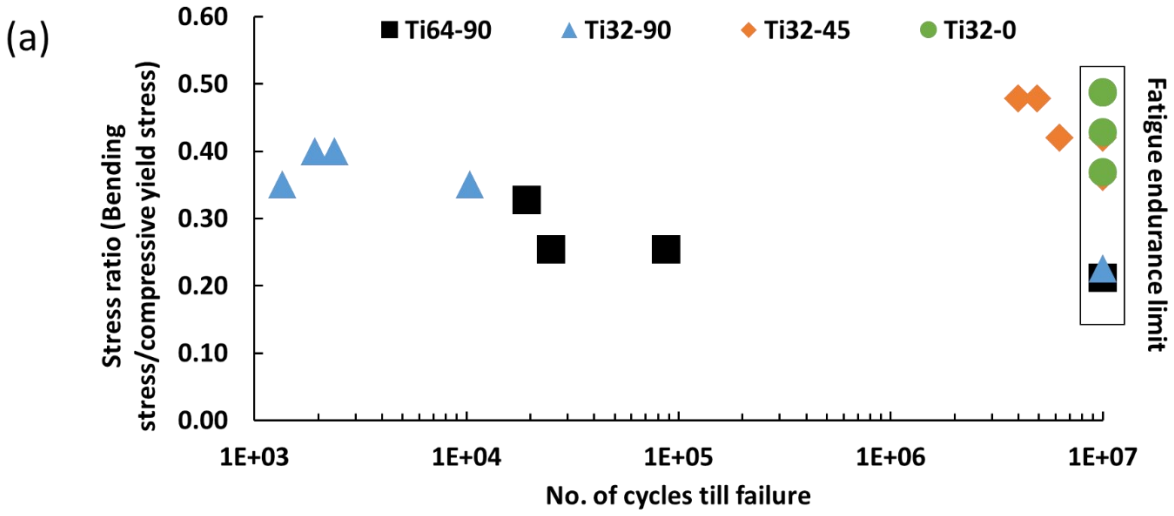
(a)
Ti64-90
Ti32-90
Ti32-45
Ti32-0
Stress ratio (Bending stress/compressive yield stress)
0.60
0.50
0.40
0.30
0.20
0.10
0.00
1E+03
1E+04
1E+05
1E+06
1E+07
No. of cycles till failure
Fatigue endurance limit

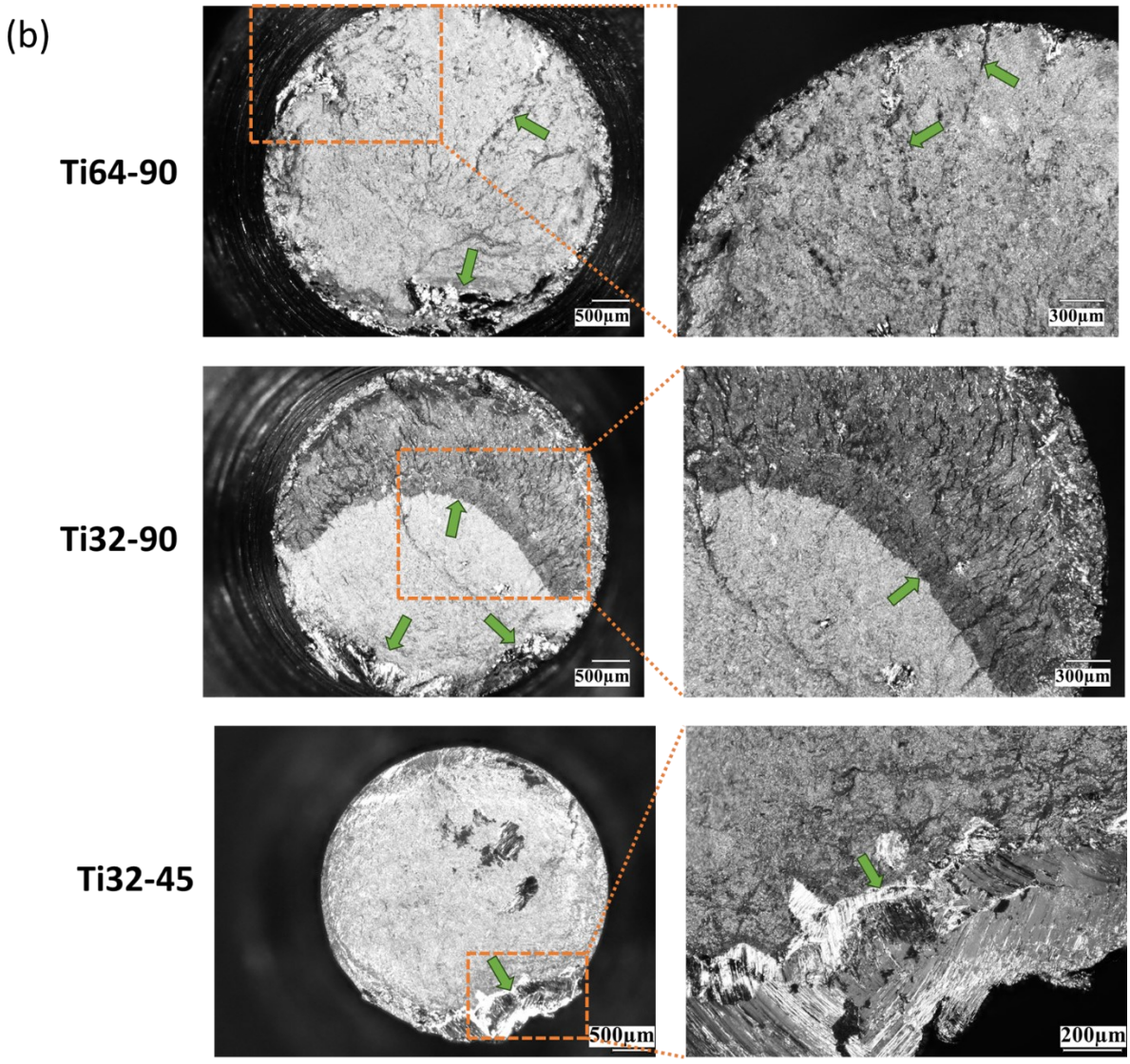
(b)
Ti64-90
Ti32-90
Ti32-45
500μm
300μm
500μm
300μm
500μm
200μm

1

Fig. 4. (a) High cycle fatigue plot for Ti64-90 and Ti32-90/45/0 specimens at various loads. The y-axis is represented as the ratio of the bending stress applied to their respective compressive yield strengths. The endurance limit has been marked and considered as the loads for which 10 million cycles were achieved prior to failure. (b) Optical images of the fracture surfaces for Ti64-90, Ti32-90, and Ti32-45 specimens. The arrows indicate the onset of failure and crack propagation through the specimens at failure.

4. Discussion

This study implemented a novel alloy design to enhance biocompatibility for orthopedic implants to replace Ti6Al4V. The designed alloy, Ti3Al2V, with reduced amounts of Al and V contents in Ti6Al4V is expected to demonstrate good mechanical performance without significant reduction from Ti6Al4V. Implants at load-bearing sites are under a multiaxial loading condition *in vivo*. It is essential to investigate the mechanical strength assessment of such alloys, particularly under cyclic fatigue loading, to avoid fractures and implant failures *in vivo*.

Fracture initiation of specimens under cyclic loading starts at the surface of the gauge length, suggesting that higher surface roughness of the test specimens leads to early fractures. Another critical parameter is the presence of residual pores, which contributes to faster crack propagation and early failure [40]. AM-processed parts are known to possess surface roughness and the presence of residual pores in each layer due to the layer-wise nature of the process [44]–[46]. Fatigue life and endurance limit of AM-processed Ti6Al4V have been studied extensively and shown in **Table 4.** It depicts low endurance limits from various studies for L-PBF-processed Ti6Al4V. With surface roughness introduced by the L-PBF process, machining is often implemented to reduce that. In this study, L-PBF-manufactured and machined Ti6Al4V built at

90˚ orientations displayed an endurance limit of 250 MPa, similar to that observed in various studies reported in **Table 4**.

Table 4. Endurance limit for L-PBF processed Ti6Al4V with post-processing treatments from various studies.

AM technique	Post-processing	Stress amplitude ratio (R)	Endurance limit (MPa)	Reference
L-PBF	As-printed, machined	-1	220	[47]
	As-printed	0.1	350	[48]
	Heat-treated, machined	0.1	400	[49]
	As-printed	-0.2	210	[50]
	As-printed, polished	-1	250	[40]

Surface roughness is critical in preventing crack propagation and enhancing fatigue life [51], [52]. A study by Vayssette et al. investigated the fatigue performance of as-printed and machined L-PBF-built Ti6Al4V and observed the strength to reach 0.2 million cycles was 223 MPa for as-printed specimens, whereas that for machined samples was 513 MPa [53]. High cycle fatigue values for Ti6Al4V presented in **Table 3** were evaluated for test specimens machined at 1200 rpm on a CNC machine. To observe if machining parameters had any significant effect on the surface roughness and subsequently on the fatigue performance, Ti64-90 specimens were also machined at 600 rpm and tested for fatigue failure. The lowered machining rpm showed a significant effect on the fatigue life. The endurance limit for Ti64-90 increased from 250 MPa

(1200 rpm) to 300 MPa (600 rpm), with 4 million cycles observed at 500 MPa for Ti64-90 (600 rpm). **Fig. 5** represents the microscopic features on the periphery of the specimens machined at 1200 and 600 rpms. High magnification images observed at the periphery of the top surface of the fatigue specimen, **Fig. 5a**, show defects on the specimen's surface, contributing to its early failure under fatigue loading. However, the specimen machined at 600 rpm shows a clean surface with minimal to no defects present at the surface. **Fig.5b** represents high-magnification images and surface depth profiling at the gauge region. A lower degree of roughness can be observed for the specimen machined at 600 rpm, with surface depth profiling showing a more homogeneous depth distribution than at 1200 rpm. As discussed, the lower surface roughness for the 600 rpm machined Ti64-90 specimen resulted in a higher endurance limit. This indicates that machining parameters can affect surface defects and roughness, influencing fatigue performance.

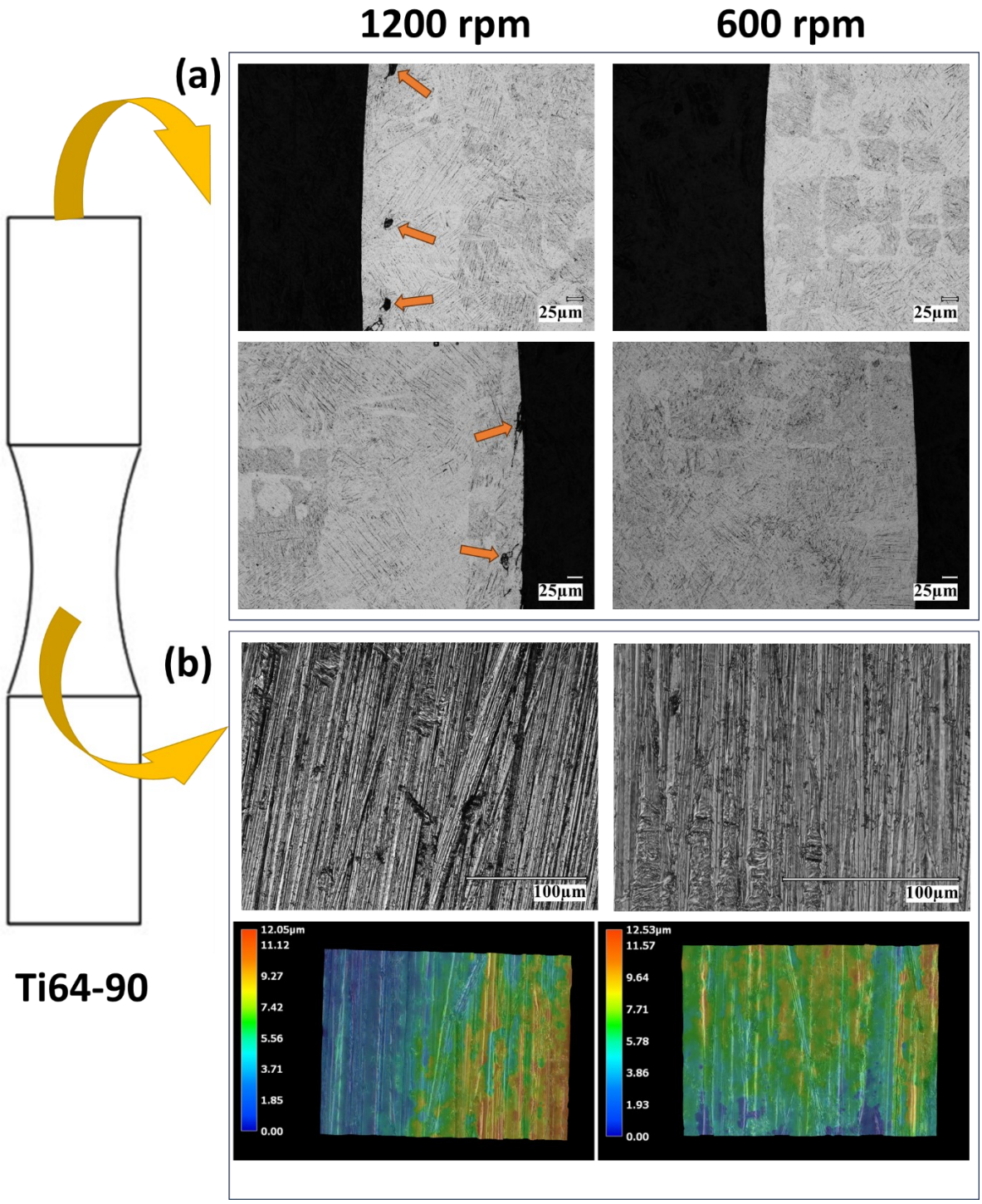

Fig. 5. Effect of machining rpm on the surface of Ti46-90 fatigue specimens; (a) reports high magnification images of the top surface of the fatigue specimens with machined surfaces at 1200 and 600 rpm. Defects are observed on the periphery of the surface of samples machined at 1200

rpm, while those machined at 600 rpm show a clean outer surface. (b) reports high magnification images of the gauge region of the fatigue specimens post-machining and depth profiling representing the surface roughness. Fatigue specimens machined at 1200 rpm display rugged surfaces with depth profiling indicating large variation in depths at the gauge region, indicating higher surface roughness. Specimen machined at a lower speed of 600 rpm exhibit lower ruggedness at the gauge area, with surface depth profiling indicating a more uniform pattern and a lower surface roughness than that for 1200 rpm specimen.

The excellent fatigue resistance of Ti6Al4V is due to the presence of the alloying elements Al and V. The endurance limit is expected to reduce with a reduced amount of alloying elements. The fatigue limit was observed to be lowered to 219 MPa for Ti3Al2V specimens built at 90˚ orientation. It is to be noted that the ratio of the compressive yield strength and endurance limit of these compositions is the same (0.21 for Ti64-90 vs. 0.23 for Ti32-90), suggesting the only factor contributing towards reduced endurance limit is the reduction in the alloying elements. With a reduction in the build orientation, the number of layers in processing the specimens is reduced, which reduces the residual porosities introduced between subsequent layers as can be seen from microstructural images, **Fig. 2**; Ti32-90 shows interlayer lack of fusion pores, which contribute toward their lower endurance limit than Ti32-45 and Ti32-0. For Ti32-45, the endurance limit was 387.5 MPa, which exceeds that of Ti64-90. With further reduction in build orientation, Ti32-0 displayed the highest endurance limit of 512.5 MPa, more than twice that for Ti64-90. This endurance limit of 512.5 MPa for Ti32-0 was similar to that of wrought-heat-treated Ti6Al4V of ~500 MPa in a study by Janeček et al. [54]. The heat treatment conducted in this study at 400˚ C was to relieve stresses with retainment of fine α' grains. Heat treatments of Ti6Al4V above its β transus temperature (995˚ C) have been shown to enhance

further the fatigue performance due to the transformation of martensitic α' to homogeneously distributed α+β microstructure [37]. Although the compressive yield strength did not show a significant effect of build orientation for Ti3Al2V alloy, the effect on the fatigue performance was apparent. The reduced Al and V chemistry in Ti3Al2V did not result in significant differences in fatigue behavior and can potentially be used in orthopedic implants.

5. Conclusions

Commercially pure titanium (CpTi) exhibits better biocompatibility over Ti6Al4V but lacks strength and fatigue resistance. A novel alloy design is implemented in this study by reducing the Al and V contents in Ti6Al4V to design Ti3Al2V, an intermediate alloy between CpTi and Ti6Al4V. This alloy was designed specifically for orthopedic applications and is expected to exhibit no significant reduction in mechanical performance compared to Ti6Al4V. Additive manufacturing was implemented to process Ti6Al4V and Ti3Al2V compositions.

- Tensile tests revealed an ultimate tensile strength of 989 MPa for Ti3Al2V, which is closer to that for Ti6Al4V (1000-1100 MPa) from various studies.
- Compressive yield strength reduction of 18% was observed in Ti3Al2V (968 ± 24 MPa) compared to Ti6Al4V (1178 ± 33 MPa) built at 90° orientation to the build plate.
- To observe the effects of build direction accounting for anisotropy, Ti3Al2V specimens built at 45° and 0° displayed an increase in compressive yield strength; however, no significant difference was observed between the 45° (1071 ± 16 MPa) and 0° (1051 ± 18 MPa) Ti3Al2V.
- Fatigue specimens built at 90° orientation exhibited an endurance limit of 250 MPa for Ti6Al4V and 219 MPa for Ti3Al2V, reaching 10 million cycles without failure, with the

ratios of bending stress applied to their respective compressive yield strengths being similar (0.21 vs. 0.23, respectively).

- The effect of build orientation for Ti3Al2V specimens on the fatigue behavior was noticeable; the endurance limit increased more than 2-fold for specimens built at 0° for Ti3Al2V (512 MPa).

Our results show the potential of Ti3Al2V alloy for orthopedic device applications with high strength and excellent fatigue performance despite a reduced amount of the Al and V than in Ti6Al4V.

6. Acknowledgments

The authors would like to acknowledge financial support from the National Science Foundation under Grant Number CMMI 1934230. The research results reported in this publication are supported by the National Institute of Arthritis and Musculoskeletal and Skin Diseases of the National Institutes of Health under Award Numbers R01 AR067306 and R01 AR078241. The content is solely the responsibility of the authors and does not necessarily represent the official views of the National Institutes of Health.

7. Declaration of Interest

The authors declare no conflict of interest.

8. References

[1] S. Bose, D. Ke, H. Sahasrabudhe, and A. Bandyopadhyay, "Additive manufacturing of biomaterials," *Progress in Materials Science*, vol. 93, pp. 45–111, Apr. 2018, doi: 10.1016/j.pmatsci.2017.08.003.

[2] A. Bandyopadhyay, I. Mitra, J. D. Avila, M. Upadhyayula, and S. Bose, "Porous metal implants: Processing, properties, and challenges," *Int. J. Extrem. Manuf.*, 2023, doi: 10.1088/2631-7990/acdd35.

[3] L.-Y. Chen, Y.-W. Cui, and L.-C. Zhang, "Recent Development in Beta Titanium Alloys for Biomedical Applications," *Metals*, vol. 10, no. 9, Art. no. 9, Sep. 2020, doi: 10.3390/met10091139.

[4] A. Bandyopadhyay, K. D. Traxel, M. Lang, M. Juhasz, N. Eliaz, and S. Bose, "Alloy design via additive manufacturing: Advantages, challenges, applications and perspectives," *Materials Today*, vol. 52, pp. 207–224, Jan. 2022, doi: 10.1016/j.mattod.2021.11.026.

[5] S. Liu and Y. C. Shin, "Additive manufacturing of Ti6Al4V alloy: A review," *Materials & Design*, vol. 164, p. 107552, Feb. 2019, doi: 10.1016/j.matdes.2018.107552.

[6] S. Ciliveri and A. Bandyopadhyay, "Understanding the influence of alloying elements on the print quality of powder bed fusionbased metal additive manufacturing: Ta and Cu addition to Ti alloy," *Virtual and Physical Prototyping*, doi: 10.1080/17452759.2023.2248464.

[7] C. Han, C. B. Johansson, A. Wennerberg, and T. Albrektsson, "Quantitative and qualitative investigations of surface enlarged titanium and titanium alloy implants," *Clinical Oral Implants Research*, vol. 9, no. 1, pp. 1–10, 1998, doi: 10.1034/j.1600-0501.1998.090101.x.

[8] C. B. Johansson, J. Lausmaa, T. Röstlund, and P. Thomsen, "Commercially pure titanium and Ti6AI4V implants with and without nitrogen-ion implantation: surface characterization and quantitative studies in rabbit cortical bone," *J Mater Sci: Mater Med*, vol. 4, no. 2, pp. 132–141, Mar. 1993, doi: 10.1007/BF00120382.

[9] S. Amin Yavari *et al.*, "Fatigue behavior of porous biomaterials manufactured using selective laser melting," *Materials Science and Engineering: C*, vol. 33, no. 8, pp. 4849–4858, Dec. 2013, doi: 10.1016/j.msec.2013.08.006.

[10] A. Bandyopadhyay, M. Upadhyayula, K. D. Traxel, and B. Onuike, "Influence of deposition orientation on fatigue response of LENS^{TM} processed Ti6Al4V," *Materials Letters*, vol. 255, p. 126541, Nov. 2019, doi: 10.1016/j.matlet.2019.126541.

[11] M. Benedetti, M. Cazzolli, V. Fontanari, and M. Leoni, "Fatigue limit of Ti6Al4V alloy produced by Selective Laser Sintering," *Procedia Structural Integrity*, vol. 2, pp. 3158–3167, Jan. 2016, doi: 10.1016/j.prostr.2016.06.394.

[12] I. Mitra *et al.*, "3D Printing in alloy design to improve biocompatibility in metallic implants," *Materials Today*, vol. 45, pp. 20–34, May 2021, doi: 10.1016/j.mattod.2020.11.021.

[13] A. Bandyopadhyay, F. Espana, V. K. Balla, S. Bose, Y. Ohgami, and N. M. Davies, "Influence of porosity on mechanical properties and in vivo response of Ti6Al4V implants," *Acta Biomaterialia*, vol. 6, no. 4, pp. 1640–1648, Apr. 2010, doi: 10.1016/j.actbio.2009.11.011.

[14] A. Bandyopadhyay, I. Mitra, S. B. Goodman, M. Kumar, and S. Bose, "Improving biocompatibility for next generation of metallic implants," *Progress in Materials Science*, vol. 133, p. 101053, Mar. 2023, doi: 10.1016/j.pmatsci.2022.101053.

[15] S. L. Sing, "Perspectives on Additive Manufacturing Enabled Beta- Titanium Alloys for Biomedical Applications," *International Journal of Bioprinting*, vol. 8, no. 1, Jan. 2022, doi: 10.18063/ijb.v8i1.478.

[16] T. Zhang and C.-T. Liu, "Design of titanium alloys by additive manufacturing: A critical review," *Advanced Powder Materials*, vol. 1, no. 1, p. 100014, Jan. 2022, doi: 10.1016/j.apmate.2021.11.001.

[17] C.-W. Lin, C.-P. Ju, and J.-H. Chern Lin, "A comparison of the fatigue behavior of cast Ti–7.5Mo with c.p. titanium, Ti–6Al–4V and Ti–13Nb–13Zr alloys," *Biomaterials*, vol. 26, no. 16, pp. 2899–2907, Jun. 2005, doi: 10.1016/j.biomaterials.2004.09.007.

[18] T. Akahori, M. Niinomi, H. Fukui, M. Ogawa, and H. Toda, "Improvement in fatigue characteristics of newly developed beta type titanium alloy for biomedical applications by thermo-mechanical treatments," *Materials Science and Engineering: C*, vol. 25, no. 3, pp. 248–254, May 2005, doi: 10.1016/j.msec.2004.12.007.

[19] M. Niinomi, "Mechanical biocompatibilities of titanium alloys for biomedical applications," *Journal of the Mechanical Behavior of Biomedical Materials*, vol. 1, no. 1, pp. 30–42, Jan. 2008, doi: 10.1016/j.jmbbm.2007.07.001.

[20] "Standard Specification for Wrought Titanium-13Niobium-13Zirconium Alloy for Surgical Implant Applications (UNS R58130)." https://www.astm.org/f1713-08r21e01.html (accessed May 06, 2022).

[21] W. F. Ho, C. P. Ju, and J. H. Chern Lin, "Structure and properties of cast binary Ti–Mo alloys," *Biomaterials*, vol. 20, no. 22, pp. 2115–2122, Nov. 1999, doi: 10.1016/S0142-9612(99)00114-3.

[22] S. Ciliveri and A. Bandyopadhyay, "Influence of strut-size and cell-size variations on porous Ti6Al4V coated structures for load-bearing implants," *Journal of the Mechanical Behavior of Biomedical Materials*, p. 105023, Dec. 2021, doi: 10.1016/j.jmbbm.2021.105023.

[23] A. J. Sterling, B. Torries, N. Shamsaei, S. M. Thompson, and D. W. Seely, "Fatigue behavior and failure mechanisms of direct laser deposited Ti–6Al–4V," *Materials Science and Engineering: A*, vol. 655, pp. 100–112, Feb. 2016, doi: 10.1016/j.msea.2015.12.026.

[24] A. Bandyopadhyay, Y. Zhang, and S. Bose, "Recent developments in metal additive manufacturing," *Current Opinion in Chemical Engineering*, vol. 28, pp. 96–104, Jun. 2020, doi: 10.1016/j.coche.2020.03.001.

[25] C. Chua, S. L. Sing, and C. K. Chua, "Characterisation of in-situ alloyed titanium-tantalum lattice structures by laser powder bed fusion using finite element analysis," *Virtual and Physical Prototyping*, vol. 18, no. 1, p. e2138463, Dec. 2023, doi: 10.1080/17452759.2022.2138463.

[26] J. Yang *et al.*, "Static Compressive Behavior and Material Failure Mechanism of Trabecular Tantalum Scaffolds Fabricated by Laser Powder Bed Fusion-based Additive Manufacturing," *International Journal of Bioprinting*, vol. 8, no. 1, Art. no. 1, Oct. 2021, doi: 10.18063/ijb.v8i1.438.

[27] A. Bandyopadhyay, S. Ciliveri, and S. Bose, "Metal Additive Manufacturing for Load-Bearing Implants," *J Indian Inst Sci*, Jan. 2022, doi: 10.1007/s41745-021-00281-x.

[28] A. Haleem and Mohd. Javaid, "3D scanning applications in medical field: A literature-based review," *Clinical Epidemiology and Global Health*, vol. 7, no. 2, pp. 199–210, Jun. 2019, doi: 10.1016/j.cegh.2018.05.006.

[29] 14:00-17:00, "ISO/ASTM 52909:2022," *ISO*. https://www.iso.org/standard/74639.html (accessed Aug. 16, 2023).

[30] "Standard Test Methods of Compression Testing of Metallic Materials at Room Temperature." https://www.astm.org/e0009-19.html (accessed Jan. 20, 2023).

[31] 14:00-17:00, "ISO 1143:2021," *ISO*. https://www.iso.org/standard/79575.html (accessed Sep. 10, 2023).

[32] 14:00-17:00, "ISO 5832-3:2021," *ISO*. https://www.iso.org/standard/79626.html (accessed Jul. 23, 2023).

[33] B. E. Carroll, T. A. Palmer, and A. M. Beese, "Anisotropic tensile behavior of Ti–6Al–4V components fabricated with directed energy deposition additive manufacturing," *Acta Materialia*, vol. 87, pp. 309–320, Apr. 2015, doi: 10.1016/j.actamat.2014.12.054.

[34] F. Wang, J. Mei, H. Jiang, and X. Wu, "Laser fabrication of Ti6Al4V/TiC composites using simultaneous powder and wire feed," *Materials Science and Engineering: A*, vol. 445–446, pp. 461–466, Feb. 2007, doi: 10.1016/j.msea.2006.09.093.

[35] J. Alcisto *et al.*, "Tensile Properties and Microstructures of Laser-Formed Ti-6Al-4V," *J. of Materi Eng and Perform*, vol. 20, no. 2, pp. 203–212, Mar. 2011, doi: 10.1007/s11665-010-9670-9.

[36] G. P. Dinda, L. Song, and J. Mazumder, "Fabrication of Ti-6Al-4V Scaffolds by Direct Metal Deposition," *Metall Mater Trans A*, vol. 39, no. 12, pp. 2914–2922, Dec. 2008, doi: 10.1007/s11661-008-9634-y.

[37] H. Galarraga, R. J. Warren, D. A. Lados, R. R. Dehoff, M. M. Kirka, and P. Nandwana, "Effects of heat treatments on microstructure and properties of Ti-6Al-4V ELI alloy fabricated by electron beam melting (EBM)," *Materials Science and Engineering: A*, vol. 685, pp. 417–428, Feb. 2017, doi: 10.1016/j.msea.2017.01.019.

[38] B. Wysocki, P. Maj, R. Sitek, J. Buhagiar, K. J. Kurzydłowski, and W. Święszkowski, "Laser and Electron Beam Additive Manufacturing Methods of Fabricating Titanium Bone Implants," *Applied Sciences*, vol. 7, p. 657, Jun. 2017, doi: 10.3390/app7070657.

[39] P. Edwards, A. O'Conner, and M. Ramulu, "Electron Beam Additive Manufacturing of Titanium Components: Properties and Performance," *Journal of Manufacturing Science and Engineering*, vol. 135, no. 061016, Nov. 2013, doi: 10.1115/1.4025773.

[40] V. Chastand, P. Quaegebeur, W. Maia, and E. Charkaluk, "Comparative study of fatigue properties of Ti-6Al-4V specimens built by electron beam melting (EBM) and selective laser melting (SLM)," *Materials Characterization*, vol. 143, pp. 76–81, Sep. 2018, doi: 10.1016/j.matchar.2018.03.028.

[41] D. A. Hollander *et al.*, "Structural, mechanical and in vitro characterization of individually structured Ti–6Al–4V produced by direct laser forming," *Biomaterials*, vol. 27, no. 7, pp. 955–963, Mar. 2006, doi: 10.1016/j.biomaterials.2005.07.041.

[42] L. Facchini, E. Magalini, P. Robotti, A. Molinari, S. Höges, and K. Wissenbach, "Ductility of a Ti-6Al-4V alloy produced by selective laser melting of prealloyed powders," *Rapid Prototyping Journal*, vol. 16, no. 6, pp. 450–459, Jan. 2010, doi: 10.1108/13552541011083371.

[43] T. Vilaro, C. Colin, and J. D. Bartout, "As-Fabricated and Heat-Treated Microstructures of the Ti-6Al-4V Alloy Processed by Selective Laser Melting," *Metall Mater Trans A*, vol. 42, no. 10, pp. 3190–3199, Oct. 2011, doi: 10.1007/s11661-011-0731-y.

[44] W. Yu *et al.*, "Processing and characterization of crack-free 7075 aluminum alloys with elemental Zr modification by laser powder bed fusion," *Materials Science in Additive Manufacturing*, vol. 1, no. 1, Art. no. 1, Mar. 2022, doi: 10.18063/msam.v1i1.4.

[45] X. Zhang *et al.*, "Influence of erbium addition on the defects of selective laser-melted 7075 aluminium alloy," *Virtual and Physical Prototyping*, vol. 17, no. 2, pp. 406–418, Apr. 2022, doi: 10.1080/17452759.2021.1990358.

[46] S. L. Sing *et al.*, "Emerging metallic systems for additive manufacturing: In-situ alloying and multi-metal processing in laser powder bed fusion," *Progress in Materials Science*, vol. 119, p. 100795, Jun. 2021, doi: 10.1016/j.pmatsci.2021.100795.

[47] K. Mertova, J. Dzugan, and M. Roudnicka, "Fatigue properties of SLM-produced Ti6Al4V with various post-processing processes," *IOP Conf. Ser.: Mater. Sci. Eng.*, vol. 461, no. 1, p. 012052, Dec. 2018, doi: 10.1088/1757-899X/461/1/012052.

[48] H. Gong, K. Rafi, H. Gu, G. D. Janaki Ram, T. Starr, and B. Stucker, "Influence of defects on mechanical properties of Ti–6Al–4V components produced by selective laser melting and electron beam melting," *Materials & Design*, vol. 86, pp. 545–554, Dec. 2015, doi: 10.1016/j.matdes.2015.07.147.

[49] W. Xu, S. Sun, J. Elambasseril, Q. Liu, M. Brandt, and M. Qian, "Ti-6Al-4V Additively Manufactured by Selective Laser Melting with Superior Mechanical Properties," *JOM*, vol. 67, no. 3, pp. 668–673, Mar. 2015, doi: 10.1007/s11837-015-1297-8.

[50] P. Edwards and M. Ramulu, "Fatigue performance evaluation of selective laser melted Ti–6Al–4V," *Materials Science and Engineering: A*, vol. 598, pp. 327–337, Mar. 2014, doi: 10.1016/j.msea.2014.01.041.

[51] A. Fatemi, R. Molaei, S. Sharifimehr, N. Phan, and N. Shamsaei, "Multiaxial fatigue behavior of wrought and additive manufactured Ti-6Al-4V including surface finish effect," *International Journal of Fatigue*, vol. 100, pp. 347–366, Jul. 2017, doi: 10.1016/j.ijfatigue.2017.03.044.

[52] J. Pegues, M. Roach, R. Scott Williamson, and N. Shamsaei, "Surface roughness effects on the fatigue strength of additively manufactured Ti-6Al-4V," *International Journal of Fatigue*, vol. 116, pp. 543–552, Nov. 2018, doi: 10.1016/j.ijfatigue.2018.07.013.

[53] B. Vayssette, N. Saintier, C. Brugger, M. Elmay, and E. Pessard, "Surface roughness of Ti-6Al-4V parts obtained by SLM and EBM: Effect on the High Cycle Fatigue life," *Procedia Engineering*, vol. 213, pp. 89–97, Jan. 2018, doi: 10.1016/j.proeng.2018.02.010.

[54] M. Janeček *et al.*, "The Very High Cycle Fatigue Behaviour of Ti-6Al-4V Alloy," *Acta Physica Polonica A*, vol. 128, pp. 497–503, Oct. 2015, doi: 10.12693/APhysPolA.128.497.